JOURNAL OF PROPULSION AND POWER
Vol. 26, No. 3, May–June 2010

Raman Scattering Measurements of Gaseous Ethylene Jets in Mach 2 Supersonic Crossflow

Kuo-Cheng Lin*
Taitech, Inc., Beavercreek, Ohio 45430
Michael Ryan†
Universal Technology Corporation, Beavercreek, Ohio 45432
and
Campbell Carter,‡ Mark Gruber,§ and Charbel Raffoul¶
U.S. Air Force Research Laboratory, Wright–Patterson Air Force Base, Ohio 45433

DOI: 10.2514/1.43757

The structures of sonic ethylene jets delivered from orifices of three different diameters and two injection angles (30 and 90 deg) into a Mach 2 supersonic crossflow were studied experimentally. The ratio of the cross-sectional areas of the largest and smallest injectors is 25:1. Time-averaged spontaneous vibrational Raman scattering was used to quantify injectant concentrations by constructing two-dimensional spanwise concentration images from the one-dimensional linewise Raman scattering images. Based on the present data set, new penetration height correlations were developed to treat cases with injection angles of both 30 and 90 deg. Excluding the influence of wall boundary layer, the present measurements show that the properties of fuel plume structures, such as shape, size, and concentration profiles, are scalable with the injector size. The measured ethylene concentrations were also compared with predictions from the revised jet penetration code, which was calibrated primarily with hydrogen and helium. Discrepancies were observed between the measurements and the jet penetration code predictions for the structures of ethylene fuel plumes. The experimental data generated from the present study can be used to validate the numerical simulations.

Nomenclature

d	=	injector orifice diameter, also d_0
d_{eff}	=	effective diameter
h	=	fuel plume penetration height
M	=	Mach number
P_0	=	total pressure
q	=	jet-to-air momentum flux ratio, $(\rho v^2)_j/(\rho v^2)_\infty$
r	=	effective radius of injector orifice
T_0	=	total temperature
v	=	velocity
x	=	freestream direction
X_i	=	mole fraction of species i
y	=	transverse direction
z	=	spanwise direction
θ	=	injection angle relative to the freestream air
ρ	=	density

Subscripts

j	=	property of the injectant
0.01	=	property defined at a mole fraction of 0.01
∞	=	freestream condition

Introduction

THE delivery of gaseous fuel into a supersonic crossflow is an important aspect of high-speed air-breathing combustors, which require efficient fuel–air mixing due to the short residence time within the engine. The properties of the injected fuel plume, such as penetration height, plume size, and concentration profiles, play important roles in dictating ignition, flame holding, flame spreading, and combustion efficiency for a given flowpath. The selection of injector type, injector placement, and number of injectors is one of the crucial engineering decisions in designing a robust high-speed air-breathing combustor flowpath. Ideally, the injection scheme should achieve the desired fuel–air mixing with minimal stagnation pressure loss. Several existing papers provide extensive reviews on fuel-injection technologies associated with the development of high-speed, air-breathing propulsion technology [1–4].

The flush-wall injector has been a fairly simple response to the challenge of fueling a high-speed air-breathing combustor. Flush-wall injectors can be directly drilled on the combustor walls or be distributed on the surface of intrusive injection components, such as struts and pylons. In addition to the injector placement and operating conditions, the design space for a flush-wall injector includes the choice of fuel, orifice shape, orifice size, and injection angle. Properties of injected gas plumes from several types of flush-wall injectors have been investigated to generate a broad range of data and to obtain useful insights into fundamental fuel–air mixing mechanisms [3–13]. Furthermore, useful correlations, predictive tools, and sophisticated numerical simulation capabilities have been developed to model the gaseous fuel jets to facilitate combustor design and to supplement limited testing opportunities.

The applicability of the existing correlations and predictive tools to a large-scale, high-speed air-breathing propulsion flowpath should

Presented as Paper 1423 at the 47th AIAA Aerospace Sciences Meeting and Exhibit, Orlando, FL, 5–8 January 2009; received 11 February 2009; revision received 9 February 2010; accepted for publication 12 February 2010.

*Senior Research Scientist, 1430 Oak Court, Suite 301; Kuo-Cheng.Lin@wpafb.af.mil. Associate Fellow AIAA (Corresponding Author).

†Postdoctoral Research Scientist; currently at Pratt & Whitney Rocketdyne. Member AIAA.

‡Principal Aerospace Engineer, Propulsion Sciences Branch. Associate Fellow AIAA.

§Aerospace Engineer, Propulsion Sciences Branch. Associate Fellow AIAA.

¶Aerospace Engineer, Propulsion Technology Branch. Member AIAA.

also be further validated. This task, however, cannot be performed without expanding the existing database using relatively large injector orifices. If a high-speed air-breathing combustor is *photo scaled* in size to capture 10 times the air mass flow rate, the injector diameter should roughly be scaled up 3.2 times (square root of 10). The size of large-scale flush-wall injectors can, therefore, lie outside the typical range of injector sizes used for the development of existing correlations. Consequently, the structures of large-scale fuel plumes may not be modeled accurately by existing correlations and predictive tools. One of the contributing factors may come from the differences in the wall boundary layer, which may not be scalable between the small- and large-scale flowpaths but can greatly affect the structures of injected fuel plumes.

Among the predictive tools, the jet penetration analysis code (JETPEN) is relatively robust and easy to use. This code was first developed by Billig et al. [12] in 1971 for the analysis of gaseous jets in supersonic crossflows. The fundamental idea of this analysis is to relate the behaviors of transverse jets injected into supersonic crossflows to the behaviors of underexpanded jets injected into a quiescent environment by modeling the effective backpressure experienced by the transverse jets. The performance of the JETPEN code was later improved by Billig and Schetz [13], so that cases with injection angles other than 90 deg could be treated and the turbulent entrainment of freestream air into the fuel plume could be incorporated. The revised JETPEN code was developed over a wide range of conditions: freestream air, $1.4 \leq M_\infty \leq 6.0$; jet Mach number, $1.0 \leq M_j \leq 1.8$; injection angle, 15 deg $\leq \theta \leq$ 90 deg; jet-to-air momentum flux ratio, $1.0 \leq q \leq 10$; and helium and hydrogen injected into air. The applicability of the JETPEN code to higher-molecular-weight gases, such as hydrocarbon fuels, should be validated.

The objective of this study is to obtain quantitative fuel plume data for ethylene jets delivered from injectors of a wide range of sizes, with the largest injector orifice corresponding to a large-scale combustor. The Raman scattering technique has been implemented in several fuel–air mixing studies [14,15] and was adopted to obtain time-averaged cross-sectional concentration profiles at various freestream locations of the ethylene plumes in the present study. Other measurement approaches, notably planar laser-induced fluorescence (of nitric oxide, for example), enable the measurement of the instantaneous plume structure, but the focus here was on quantitative measurements (albeit, time averaged) that could used for model development and validation. The data will then be compared with the existing correlations for fuel plume penetration height and with the fuel plume properties predicted by the JETPEN code. The scalability of the ethylene fuel plumes will also be discussed. Ultimately, it is our hope that this database can be used for the validation of advanced numerical codes, such as those employing the large-eddy simulation technique.

Experimental Methods

Experimental Setup

Ethylene injection from various injector blocks into a Mach 2 supersonic environment was carried out in Research Cell 19 at Wright–Patterson Air Force Base (Aerospace Propulsion Division, Propulsion Directorate). The test section of the wind tunnel has a constant cross-sectional area with a width of 15.2 cm (6 in.) and a height of 13.1 cm (5.16 in.). The sidewalls have integral fused silica windows, whereas the top wall includes a BK-7 window. The total temperature and total pressure of the wind-tunnel air were kept at 300 K (80°F) and 0.24 MPa (35 psia), respectively, for the present experiment. The axis of the injector orifice was positioned at the centerline in the spanwise direction and located 15.0 cm (5.9 in.) from the entrance of the test section. The boundary-layer thickness is about 6.4 mm (0.25 in.) at the injector exit. The relatively thick wall boundary layer is more representative of the local conditions inside a large-scale flowpath. The turbulence level of the incoming freestream air into the test section was not characterized for this study but is believed to be low (<1%) based on measurements in a similar flowpath. In addition, no major flow distortion has been observed during the use of this wind tunnel for other research activities. Six injector blocks were designed and fabricated for this study. Figure 1 shows a schematic of one of these blocks. Three orifice diameters of 1.6, 4.8, and 7.9 mm (1/16, 3/16, and 5/16 in.) and two injection angles of 30 and 90 deg were selected. The ratio of the cross-sectional areas of the largest and smallest injectors is 25:1. For the 30 deg injectors, the orifice diameter refers to the diameter of the final passage before the exit orifice, which is elliptical in shape. Adapted from the injector design of Gruber et al. [11], a third-order polynomial equation was used to generate the interior contour that determines the transition from a supply tubing diameter of 19 mm (0.75 in.) to the desired injector exit diameter. The injector block is 31.8 mm (1.25 in.) thick. The inner contour was machined and polished to a smooth finish.

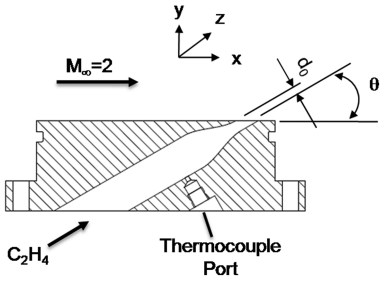

Fig. 1 Schematic of the injector block.

Injectant

Ethylene was selected as the test fluid because it represents a product of decomposed heavy hydrocarbon fuels, has a molecular weight (28) similar to that of air, and is Raman active. The handling of ethylene, however, requires special attention. To avoid undesired liquid condensation, a fuel heater was used to raise the injectant temperature before final discharge into the wind tunnel. The ethylene temperature at the fuel plenum was maintained at 315–337 K (107–147°F), depending on the selected testing conditions. At this temperature range, it was expected that ethylene would remain in the gas phase during the injection processes. The ethylene delivery line, however, could still experience freezing, due to gas expansion from high-pressure ethylene gas bottles. This problem was mitigated by limiting the ethylene supply pressure to 4.1 MPa (600 psia).

Optical Setup

Vibrational Raman scattering was used to measure species concentrations at various axial locations. The Raman scattering setup (shown in Fig. 2) consists principally of a continuous-wave 5 W Coherent, Inc., Verdi laser, operating at 532 nm, and a Kaiser Optical Systems, Inc., HoloSpec^{TM} f/1.8 holographic imaging spectrometer, both of which were mounted on a large three-axis translation table beneath the wind tunnel. In this setup, the laser beam was focused with a 1 m focal length lens into the test section, perpendicular to the direction of flow (tunnel spanwise dimension), whereas polarization of the beam was set to horizontal. Scattering from the laser beam was transmitted through the top tunnel window, reflected with a 45 deg mirror, collected and focused (on a 1-mm-wide by 7-mm-long entrance slit) with a 58 mm focal length Nikon camera lens, and dispersed within the spectrometer. To further suppress background scattering at 532 nm, a Schott glass OG 570 filter was placed in front of the collection lens. Focus of the Raman lines was optimized with the Nikon lens focusing adjustment, and so the spectral resolution was much better than the 1 mm width of the slit. A backilluminated Andor Technology charge-coupled device (CCD) camera was mounted behind the spectrometer to detect each Raman image, which was composed of the scattering spectrum along a 48-mm-long segment of the probe laser beam. The camera array is composed of 512×512 pixels, but the array was binned to give 128 pixels in the spatial dimension and 256 pixels in the spectral dimension.

The exposure time of each image was chosen to be 20 s, which provided a good signal-to-noise ratio for the derived injectant mole

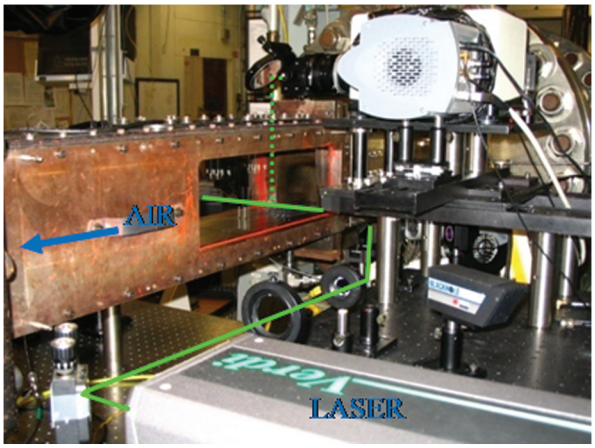

a)

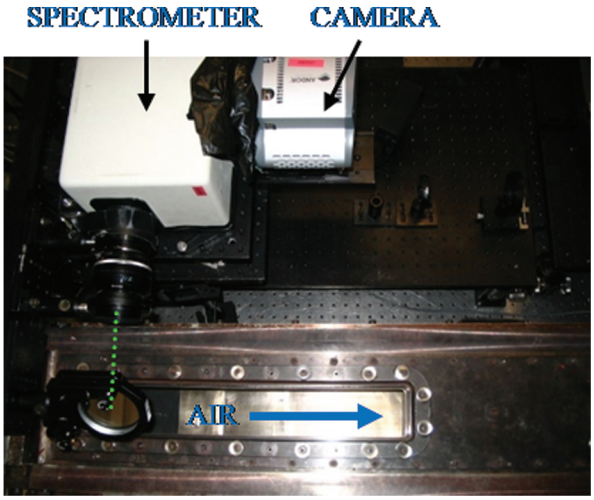

b)

Fig. 2 Optical and wind-tunnel setups: a) angle view to show laser and sending optics, and b) top view to show receiving optics. Solid green line: laser beam; dotted green line: Raman scattering signal.

fraction and a reasonable total time of about 10–15 min for each streamwise probe location. Once the laser beam was positioned at the desired freestream (x) location, the optical table was then moved to the initial location with the laser beam at the tunnel floor. The CCD array was exposed (for 20 s using the camera's mechanical shutter) and the translation table was moved 0.5 mm (∼0.02 in.) upward; the next image was then recorded. Individual 1-D images were taken at each probe height until the scattering signal from ethylene was no longer observed, and the final 2-D image was then created from the ensemble of 1-D (line) measurements. A sample raw image can be seen in Fig. 3. The horizontal direction in the image corresponds to spectral position, whereas the vertical direction corresponds to the spanwise (z) position in the wind tunnel. Three ethylene lines are present, marked E(-CH_2), E(C = C), and E(C-H) at 573–634 nm, along with oxygen and nitrogen lines at 580 and 607 nm, respectively. The ethylene scattering signal appears only in the center portion of the vertical axis of the image because ethylene is only present within the jet plume, which takes up a small portion of the field of view. A corresponding reduction in the nitrogen and oxygen signals can be seen where the ethylene signal is strongest.

The nitrogen line intensity was used to derive the air number density whereas the E(C-H) line (C-H stretch mode) was used to derive the ethylene number density. To obtain a scattering signal from the images, the background was first subtracted and then the top four pixels of each line were integrated for a total scattering signal at each spanwise location for each image. The background was modeled as a

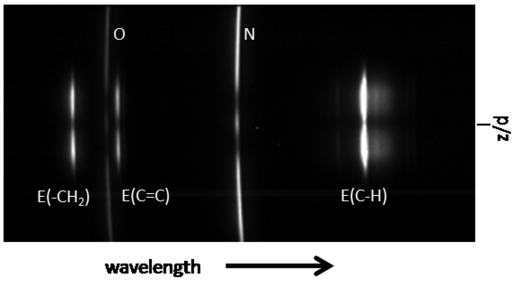

Fig. 3 Representative Raman scattering image/spectrum for an ethylene jet injected into a supersonic wind tunnel. The horizontal direction in the image corresponds to spectral position. The vertical direction corresponds to the spanwise (z) position in the wind tunnel. E(i) refer to the three principal vibrational Raman modes for ethylene.

third-order polynomial for each Raman line, for each row of each image, with intensities and slopes matched on either side of the particular Raman line. This was necessary because signals detected from scattering off the floor or particles moving through the laser beam created different background values at each position.

The Raman scattering signal is linearly proportional to species number density. In situ calibration images were taken in the tunnel without flow, at room-temperature conditions. The following procedure was used: 1) scattering from room air was recorded, 2) ethylene was injected into the tunnel and allowed to mix (thorough mixing is not required), and 3) scattering was again recorded for the mixture. The calibration factor (number density vs signal counts) for nitrogen is derived from step 1 at each location (row) along the length of the Raman line; the reduction in nitrogen signal, from step 1 to 3, allows one to calculate the ethylene number density (at each location along the Raman line), because the total number density is known from the ideal gas law (the compressibility factor is assumed to be 1). It should be noted that a loose sealing of the tunnel test section (to trap ethylene but not allow a pressure rise) was accomplished using foam at either end; tunnel temperature and pressure were monitored with the standard tunnel instrumentation to ensure that the temperature and pressure were unchanged between the two measurements. Accuracy of this calibration will depend on the noise in the two measurements of the nitrogen signal and the one of ethylene, the relative certainty of two total number densities (without and with ethylene), the overlap of the nitrogen and ethylene measurements, etc. It is estimated based on these factors that the calibration error is ±2–3%. The random error of individual ethylene mole fraction measurements appears to be as low as about ±1% of the value with large ethylene mole fractions, limited primarily by the noise in the nitrogen measurement, but will of course be greater for small values of ethylene mole fraction. As an approximate guideline, it is expected that total error magnitude will be less than 5% for ethylene mole fractions greater than the stoichiometric value (0.0636). The detection limit for the ethylene mole fraction is less than 0.1%. Once calibration values are found, the ethylene mole fraction can be calculated from each image at each spanwise location from the scattering signal. By imaging a knife edge at known spanwise locations (the knife edge was placed in the beam path and backlit), the spatial position of each pixel in both the nitrogen and the ethylene signals can be determined; this was necessary due to a slight tilt of the camera array relative to the spatial and spectral axes. Use of the knife edge also allows one to assess (and optimize, if needed) the spatial resolution of the imaging system. It should be emphasized that because mixture ratios (mole fraction, in this case) are the desired final quantity, the measurement is essentially a ratio of ethylene and nitrogen Raman signals. As such, this approach is very robust and immune to typical testing difficulties such as window fouling, laser intensity variations, etc.

Test Conditions

The test conditions are listed in Table 1. The nominal jet-to-air momentum flux ratio, q, was varied from 0.25 to 6.0. The actual test conditions deviate from the nominal injection conditions due to slight variations in tunnel and injection operating parameters. The

Table 1 Test conditions

d, mm	θ, deg	q	x/d	$P_{0,\infty}$, kPa	$T_{0,\infty}$, K	$P_{0,j}$, kPa	$T_{0,j}$, K
1.6 (1/16 in.)	90	0.49	25	242	302	123	326
			100	243	302	124	315
		1.02	25	238	302	254	321
			50	239	302	253	321
			100	239	301	254	320
		4.01	25	242	301	999	326
			100	241	302	987	324
	30	0.50	25	243	303	128	320
			100	243	302	125	315
		0.99	25	242	303	249	325
		4.06	25	242	303	1004	319
		6.00	25	243	303	1487	316
4.8 (3/16 in.)	90	0.25[a]	5	245	301	64	315
			10	245	301	64	315
			25	246	301	64	315
			51	243	301	64	315
		0.50	5	244	299	127	321
			10	244	299	128	320
			25	247	299	126	318
			50	243	299	126	320
		1.03	5	243	301	262	315
			25	243	301	258	317
		1.52	5	243	305	384	322
			25	243	303	381	323
	30	0.50	5	244	300	128	320
			10	243	300	129	318
			25	242	300	128	319
			51	242	300	125	320
		1.00	5	244	301	253	322
			25	243	301	257	317
7.9 (5/16 in.)	90	0.50	5	244	302	128	337
			15	244	302	126	331
	30				——		

[a]This condition is barely choked.

actual values in Table 1 were used as the input parameters for the JETPEN calculations and should be used for future numerical simulations. The maximum q for each injector was limited by the capacity of the fuel flowmeter. Consequently, only the $q = 0.5$ condition was carried out for the 7.9 mm (5/16 in.) injector. The test conditions were designed to generate sonic jets in the present study. The $q = 0.25$ condition for the 4.8 mm (3/16 in.) 90 deg injector, however, is barely choked with respect to the fixed total pressure of the wind tunnel, as will be discussed later. For each established injection condition, Raman scattering measurements were made at several x/d locations, to establish planar concentration contours. Because of restrictions on testing time available for the present study, the injector block with an orifice diameter of 7.9 mm (5/16 in.) and an injection angle of 30 deg was not used.

JETPEN Code

The present measurements were used to evaluate the performance of the JETPEN code. The revised JETPEN code was developed for use over a wide range of conditions: $1.4 \leq M_\infty \leq 6.0$, $1.0 \leq M_j \leq 1.8$, 15 deg $\leq \theta \leq$ 90 deg, $1.0 \leq q \leq 10$, and helium or hydrogen injected into air. Note that the use of ethylene with $q < 1$ in Table 1 is outside the calibration range for the JETPEN code. Figure 4 shows the typical prediction for fuel plume structures for one of the test conditions in Table 1. The JETPEN model returns a circular cross section for the fuel plume, as will be illustrated later, and a uniform value of the injectant mole fraction within this cross section. Depending on the nature of the prediction, the cross-sectional area can be truncated by the tunnel floor or adjacent jets, such as the region with $x/d > 32$ in Fig. 4. The National Institute of Standards and Technology's REFPROP [16] code was used to obtain heat capacities and ratios of specific heat for both freestream air and ethylene before running JETPEN. Other input parameters are the readily available operating conditions of both the wind tunnel and injector. The performance of the JETPEN code will be evaluated by comparing its predictions with the measured values in terms of plume cross-sectional area and injectant mole fraction contour.

Results and Discussion

Fuel Plume Structures

Figure 5 shows the mole fraction contours for ethylene injected at 90 deg from a 4.8 mm (3/16 in.) injector with a q of 0.5 at various axial (x/d) locations. Commercial software was used to construct the

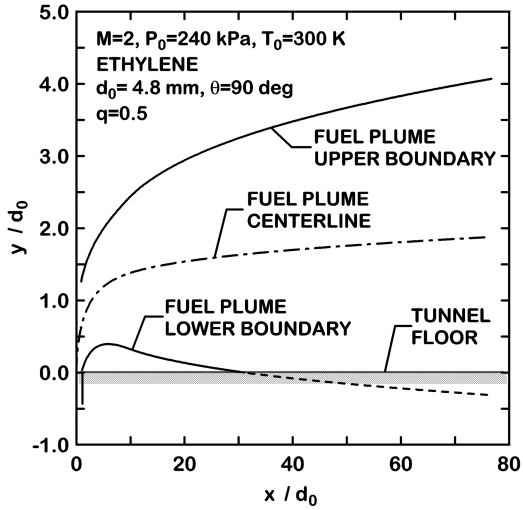

Fig. 4 Typical fuel plume structures of an ethylene jet predicted by the JETPEN code.

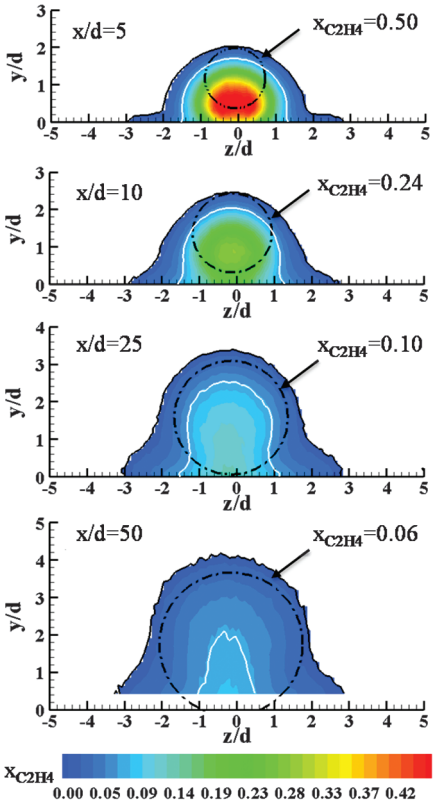

Fig. 5 Ethylene mole fraction contours for the ethylene jet injected at 90 deg from a 4.8 mm (3/16 in.) wall injector with $q = 0.5$ at various x/d locations. In the subsequent contour figures, the stoichiometry is marked with the white line and the JETPEN-predicted plume structure is marked with the dotted black line.

smooth contours from the ensemble of 1-D measurements. To better depict the size of the fuel plume, only the regions with an ethylene mole fraction greater than 0.01 are shown. Also shown in Fig. 5 are the following: the contour with the stoichiometric mole fraction (white line), the fuel plume structures predicted by the JETPEN code (dashed-dotted circle), and the JETPEN-predicted average mole fraction (within the predicted circular plume). The stoichiometric mole fraction is 0.0636 for the ethylene–air mixture. Note, however, that the present q of 0.5 is below the range of conditions ($1.0 \leq q \leq 10$) used to develop the JETPEN code. It was found that the wind tunnel is tilted slightly with respect to the x axis (freestream direction) of the translation table, as the offset from $z = 0$ to the jet center gets progressively worse further downstream. No attempt was made to correct the contour plot to account for the minor misalignment in the present study. All distances are scaled by injector diameter in Fig. 5.

The measured ethylene mole fraction contours show that the size of the fuel plume increases with the freestream distance. At the $x/d = 5$ location, some injected ethylene is distributed on both sides of the main fuel plume near the tunnel floor. There is a highly concentrated fuel core at both the $x/d = 5$ and 10 locations. The ethylene distribution becomes much more uniform as the fuel plume travels downstream. The stoichiometric line shows an initial increase in penetration height from $x/d = 5$ to 25. The plume width indicated by the stoichiometric line, however, exhibits only a minor variation. At the $x/d = 50$ location, the region enclosed by the stoichiometric line shrinks, highlighting the increase in fuel–air mixing. The comparison between the plume boundary and the stoichiometric line shows that the region with the combustible fuel–air mixture increases with the freestream distance, as the region between the stoichiometric line and the fuel plume outer boundary expands downstream. The fuel plume areas predicted by the JETPEN code are smaller than the measured values at the $x/d = 5$ and 10 locations (Fig. 5), whereas the penetration heights are in reasonable agreement. Except for the regions close to the tunnel floor, the JETPEN-predicted fuel plumes overlap the majority of the measured fuel plumes at the $x/d = 25$ and 50 locations.

Figure 6 shows the contours of the ethylene mole fraction for the ethylene jet injected from the same injector with a target q of 0.25 at various axial locations. With this injection condition, the jet is very close to being unchoked, because the calculated ethylene exit pressure (34.0 kPa with a constant specific heat ratio of 1.28) is very close to the local freestream pressure (30.7 kPa). No attempt was made to further lower the total pressure of the wind tunnel to ensure the choking condition of the jet. Nonetheless, the majority of the injected ethylene stays within the boundary layer, which, as noted earlier, has a thickness of 6.4 mm (0.25 in.) or $y/d = 1.33$ at the injection location ($x = 0$). The measured fuel plumes exhibit significant spreading in the spanwise (z) direction. As observed in Fig. 5, the stoichiometric line increases in transverse penetration initially and then disappears almost entirely at the $x/d = 50$ location. The JETPEN-predicted fuel plumes generally overlap the measured fuel plumes, except for the spanwise spreading regions. The predicted upper boundaries of the fuel plumes are close to the measured penetration height.

As the fuel flow rate is further increased to reach a q of 1.0, which matches the calibration range for JETPEN development, a significant increase in penetration height and fuel plume size can be observed in Fig. 7. At the $x/d = 5$ location, the high-concentration region exhibits a circular shape. The JETPEN code underpredicts the fuel plume size for this injection condition. Consequently, the predicted ethylene mole fractions are substantially higher than those measured. It appears that the actual fuel plume experiences a large expansion process immediately after injection, whereas the JETPEN model imposes a small expansion process for this injection condition.

For the injection condition with a q of 1.5, the distribution of high-concentration ethylene exhibits a kidney shape at the $x/d = 5$ location (Fig. 8). The kidney-shaped contour is created by the counter-rotating vortex pair. With a higher momentum flux to penetrate into the high-speed crossflow, it appears that a stronger vortex pair can be induced behind the wake region. There is only a slight increase in fuel plume size between the $q = 1.0$ and 1.5 conditions. Once again, JETPEN underpredicts the fuel plume size for the $q = 1.5$ condition.

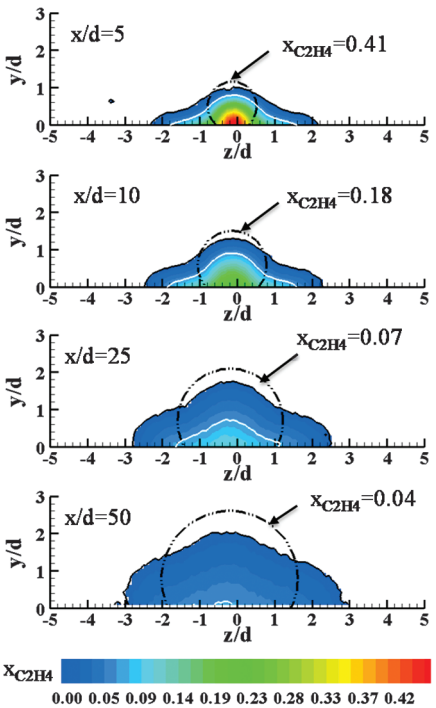

Fig. 6 Ethylene mole fraction contours for the ethylene jet injected at 90 deg from a 4.8 mm (3/16 in.) wall injector with $q = 0.25$ at various x/d locations.

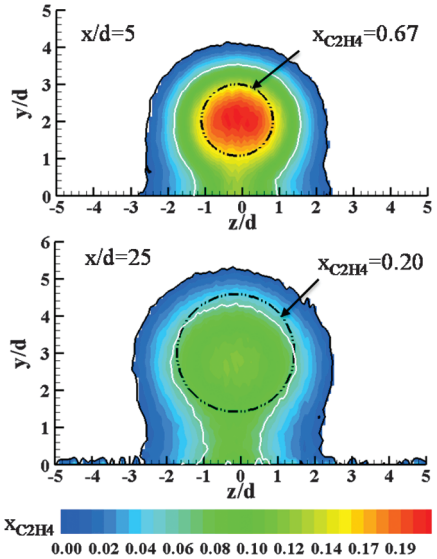

Fig. 7 Ethylene mole fraction contours for the ethylene jet injected at 90 deg from a 4.8 mm (3/16 in.) wall injector with $q = 1.0$ at various x/d locations.

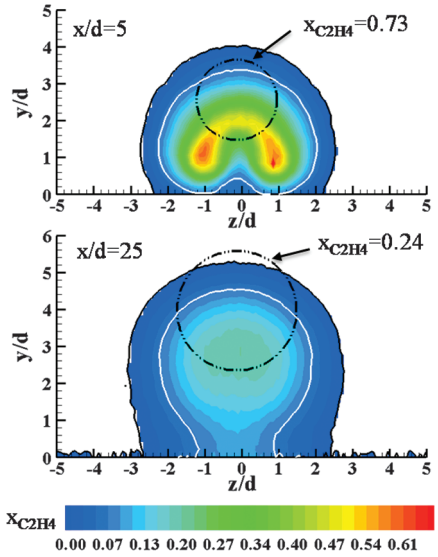

Fig. 8 Ethylene mole fraction contours for the ethylene jet injected at 90 deg from a 4.8 mm (3/16 in.) wall injector with $q = 1.5$ at various x/d locations.

The ethylene mole fraction contours at two freestream locations in Fig. 9 provide a good illustration of the effects of the momentum flux ratio and the general discrepancy between the measurements and JETPEN predictions of fuel plume structures for the four ethylene jets described earlier. The fuel plume penetration height increases with increasing q, as expected. The fuel plume width, however, is fairly insensitive to the change in q. It is interesting to point out that the fuel plume penetration heights are almost identical for the $q = 1.0$ and 1.5 cases at the two freestream locations. Also, the cross-sectional areas of the $q = 1.0$ and 1.5 fuel plumes at the $x/d = 25$ location are highly similar in Fig. 9b. It appears that the increased injection pressure (see Table 1) for the $q = 1.5$ jet does not result in

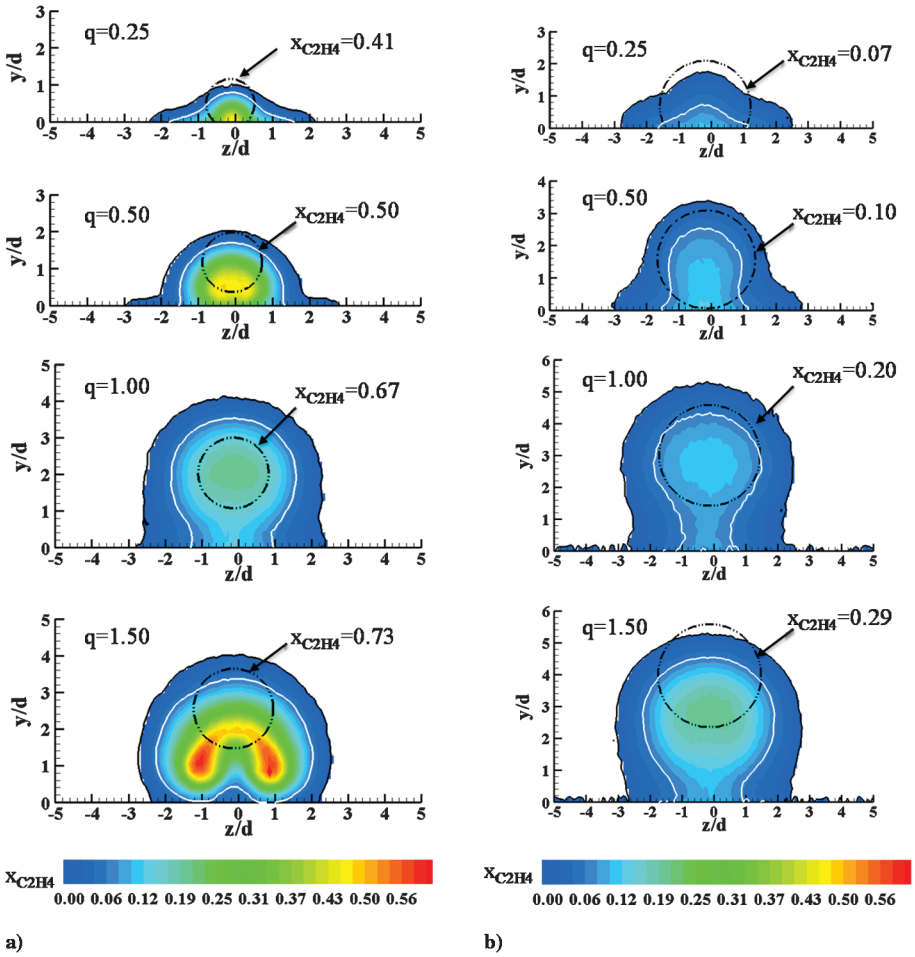

Fig. 9 Ethylene mole fraction contours for the ethylene jet injected at 90 deg from a 4.8 mm (3/16 in.) wall injector with various jet-to-air momentum flux ratios: a) $x/d = 5$, and b) $x/d = 25$.

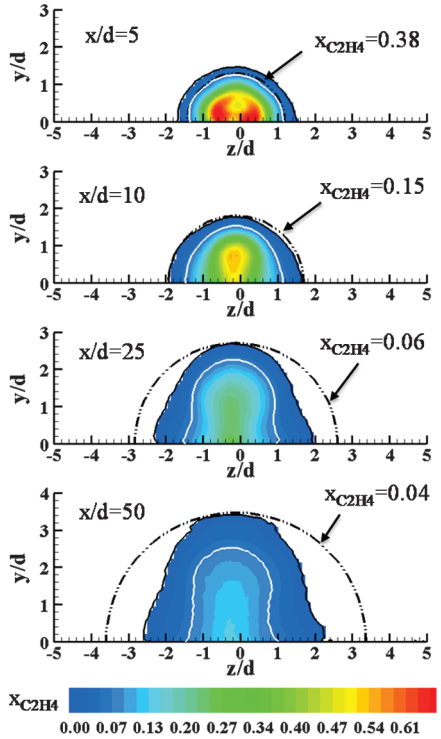

Fig. 10 Ethylene mole fraction contours for the ethylene jet injected at 30 deg from a 4.8 mm (3/16 in.) wall injector with $q = 0.5$ at various x/d locations.

an increase in plume size. Instead, a high-concentration core appears within the fuel plume for the $q = 1.5$ jet. It is hoped that the contributing mechanisms of the observed phenomena can be identified using future numerical studies, which are validated by the present quantitative measurements or future experimental investigations. The JETPEN code does a fair job of matching the actual fuel plume penetration heights but underpredicts the fuel plume size at high q conditions. With an underpredicted fuel plume size, the predicted fuel concentrations are higher than the measured values.

Figures 10 and 11 show the fuel plume structures for ethylene injected at 30 deg from a 4.8 mm (3/16 in.) injector with a q of 0.5 and 1.0, respectively. Direct comparisons between Figs. 5 and 10 for the $q = 0.5$ jet and between Figs. 7 and 11 for the $q = 1.0$ jet show that the use of a 30 deg injector delivers slightly smaller fuel penetration, lateral fuel spreading, and degree of fuel–air mixing. For instance, the portion of the region enclosed within the stoichiometric line for the 90 deg jet in Fig. 5 is smaller than that for the 30 deg jet in Fig. 10 at the $x/d = 50$ location. Also, unlike the 90 deg jet in Fig. 5, there is no injected ethylene distributed on the sides of the main fuel plume near the tunnel floor for the 30 deg jet in Fig. 10, probably due to the difference in the strength of the shock wave in front of the ethylene jet. The fuel plume exhibits a well-defined structure that is characteristic of the pair of counter-rotating vortices at the $x/d = 5$ location for the $q = 1.0$ jet in Fig. 11. This phenomenon was not observed for the $q = 1.0$ jet injected at 90 deg from the 4.8 mm (3/16 in.) injector shown in Fig. 7.

For the $q = 0.5$ jet in Fig. 10, the JETPEN prediction agrees very well with the measurement in terms of fuel plume shape at both the $x/d = 5$ and 10 locations. The agreement between the measured and predicted fuel plume penetration heights is extremely good. Unlike the conditions shown in Figs. 5–8 for the 90 deg injection angle, JETPEN overpredicts the fuel plume width at the downstream locations. Similar observations can be made for the $q = 1.0$ jet in Fig. 11. The agreement in fuel plume penetration heights in Fig. 11, however, is not as good as that in Fig. 10.

Further comparison also shows that the JETPEN code underpredicts the fuel plume size for those jets injected from the 90 deg injector, whereas it overpredicts the fuel plume size for those jets injected from the 30 deg injector at the downstream locations. At the $x/d = 25$ location, the JETPEN-predicted fuel plume size for the 30 deg jet in Fig. 11 is about 2.2 times that for the 90 deg jet in Fig. 7. The JETPEN-predicted trend obviously contradicts the experimental observations. The root causes of this discrepancy cannot be determined without a further examination of the original models employed in JETPEN.

Figure 12 shows the fuel plume structures for an ethylene jet injected at 90 deg from a 7.9 mm (5/16 in.) injector with q of 0.5 at various freestream locations. The measurements were performed up to an x/d of 15 for this injection condition. The counter-rotating vortex pair is observed at the $x/d = 3$ location in Fig. 12. Some

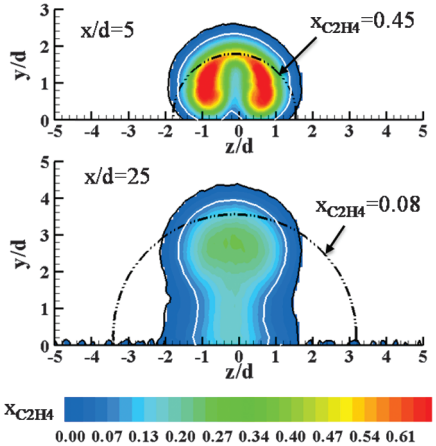

Fig. 11 Ethylene mole fraction contours for the ethylene jet injected at 30 deg from a 4.8 (3/16 in.) wall injector with $q = 1.0$ at various x/d locations.

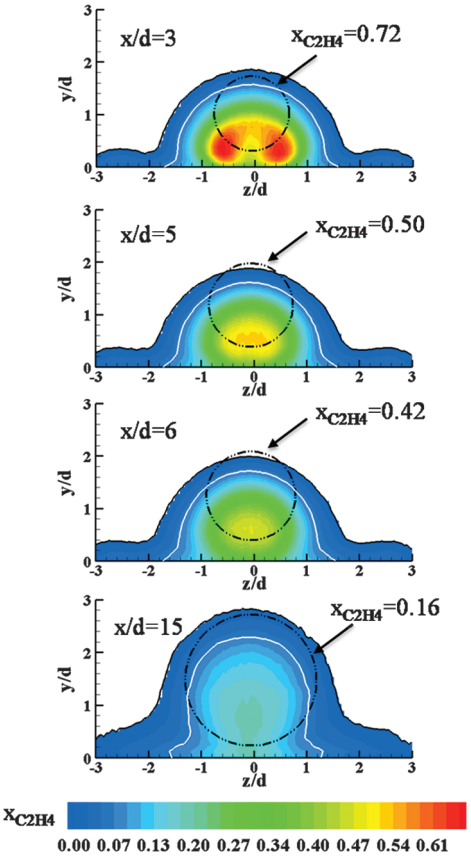

Fig. 12 Ethylene mole fraction contours for the ethylene jet injected at 90 deg from a 7.9 mm (5/16 in.) wall injector with $q = 0.5$ at various x/d locations.

injected ethylene is distributed at both sides of the main fuel plume, as observed for the 4.8 mm (3/16 in.) injector in Fig. 5. As in Fig. 5, the comparison between the measurements and JETPEN predictions in Fig. 12 also highlights the good agreement in penetration height and the underprediction in cross-sectional area at $x/d < 10$.

Results for ethylene jets injected at 90 deg from a 1.6 mm (1/16 in.) injector at various values of q are shown in Figs. 13–15. With a smaller injector orifice, the wall boundary layer, for which the thickness is 4 times the orifice diameter, is expected to affect the fuel plume structures. For the $q = 0.5$ jet in Fig. 13, the fuel plume at the $x/d = 25$ location is largely submerged inside the wall boundary layer. A similar situation can be observed for the $q = 1.0$ jet in Fig. 14. The JETPEN code, however, still gives reasonable predictions for the $q = 0.5$ jet in Fig. 13, even with the dominant influence from the relatively thick boundary layer in the present measurements. As q increases further, as illustrated in Figs. 14 and 15, the discrepancies in fuel plume structures between the measurements and JETPEN predictions increase, probably indicating that the good agreement with $q = 0.5$ is somewhat fortuitous. Although the predicted penetration height stays close to the measurement, the measured fuel plume exhibits a substantially smaller cross-sectional area with significantly less mixing with the freestream air, for a higher q condition. Note that a q of 4 (Fig. 15) lies within the calibration range ($1.0 \leq q \leq 10$) for JETPEN development.

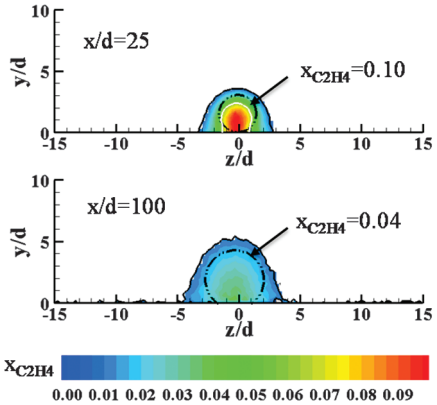

Fig. 13 Ethylene mole fraction contours for the ethylene jet injected at 90 deg from a 1.6 mm (1/16 in.) wall injector with $q = 0.5$ at various x/d locations.

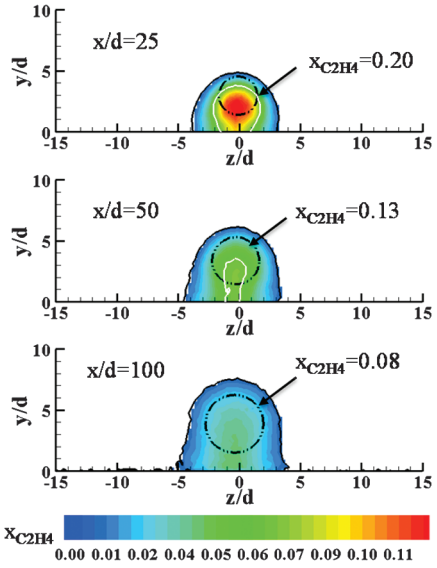

Fig. 14 Ethylene mole fraction contours for the ethylene jet injected at 90 deg from a 1.6 mm (1/16 in.) wall injector with $q = 1.0$ at various x/d locations.

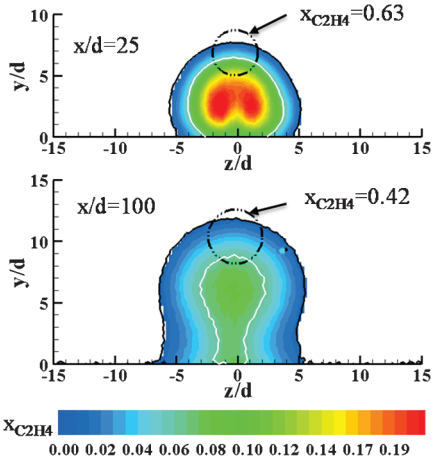

Fig. 15 Ethylene mole fraction contours for the ethylene jet injected at 90 deg from a 1.6 mm (1/16 in.) wall injector with $q = 4.0$ at various x/d locations.

For the ethylene jet injected at 30 deg from a 1.6 mm (1/16 in.) injector with a q of 0.5, the JETPEN code gives a reasonable prediction of fuel plume structures, as can be seen in Fig. 16. The slightly asymmetric plume structures in the measurements may result from defects in injector fabrication. Consequently, other results from the 30 deg injector are not discussed. Because the majority of the injected fuel is submerged inside the boundary layer, the effect of injection angle is compromised by the wall boundary layer at a low q condition, as can be seen by comparing Figs. 13 and 16. At the $x/d = 25$ location, the JETPEN-predicted fuel plume for the 30 deg jet in Fig. 16 is about 1.6 times that for the 90 deg jet in Fig. 13. Once again, this discrepancy suggests that further examination of the JETPEN code is warranted.

Fuel Plume Scalability

Scalability of fuel plume structures from injectors of different sizes has not been extensively explored so far. With the present ethylene concentration profiles from a wide range of injection conditions, the scalability and effect of the wall boundary layer on fuel plume structures can be studied. Figure 17 illustrates the similarity in shape, cross-sectional area, and concentration profiles of fuel plume structures for both $d = 4.8$ mm (3/16 in.) and $d = 7.9$ mm (5/16 in.) jets at the $x/d = 5$ location. For both jets, the effect of wall boundary layer on plume structures is believed to be small. The slight difference in the predicted ethylene mole fraction comes from the slight difference in actual injection conditions between the two jets. Figure 18 shows comparisons of plume structures between $d =$ 1.6 mm (1/16 in.) and $d = 4.8$ mm (3/16 in.) jets at two different values of q. Because of the dominant influence of the wall boundary

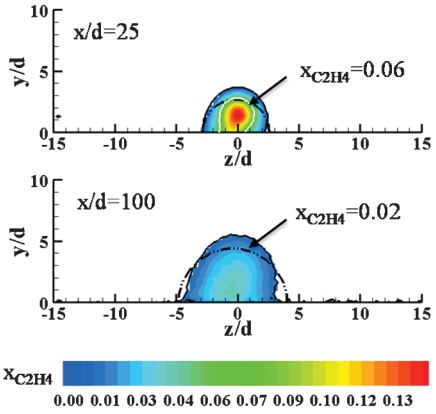

Fig. 16 Ethylene mole fraction contours for the ethylene jet injected at 30 deg from a 1.6 mm (1/16 in.) wall injector with $q = 0.5$ at various x/d locations.

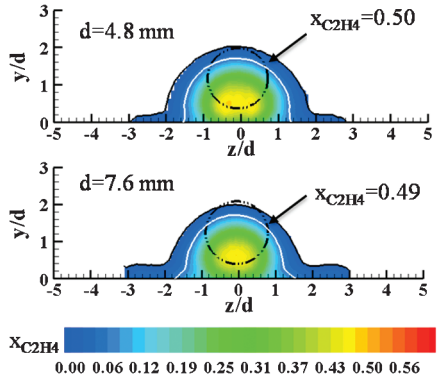

Fig. 17 Ethylene mole fraction contours for ethylene jets injected from 4.8 mm (3/16 in.) and 7.9 mm (5/16 in.) injectors with $q = 0.5$, $\theta = 90$ deg, and $x/d = 5$.

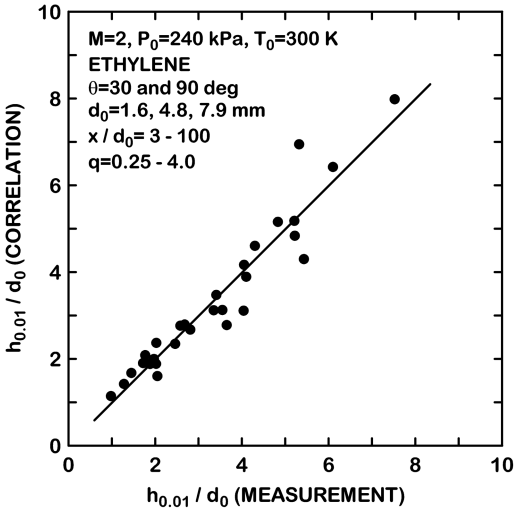

Fig. 19 Comparison of the measured penetration heights and the correlation predictions by Eq. (1) for ethylene jets in the present study.

layer on the jets injected from the 1.6 mm (1/16 in.) injector, significant differences in plume shape, especially near the tunnel floor, can be observed. Unlike the 4.8 mm (3/16 in.) jet in Fig. 18a, neither of the fuel plumes from the 1.6 mm (1/16 in.) injector exhibits fuel spillage on the tunnel floor. For the 4.8 mm (3/16 in.) jet in Fig. 18b, the lower waist of the fuel plume is pinched and the overall plume width is narrower than that of the 1.6 mm (1/16 in.) jet at the same q. Based on these observations, it is believed that the fuel plume structure is scalable with injector size as long as the majority of the fuel plume stays outside the wall boundary layer.

Fuel Plume Penetration Height

Fuel plume penetration height was obtained in the present study by using the measured ethylene mole fraction along the fuel plume centerline ($z = 0$) at various freestream locations. Based on the measured fuel plume penetration heights, $h_{0.01}$, for which an ethylene mole fraction of 0.01 was interpolated from the measurements and was used as the threshold for the definition of penetration height, a penetration height correlation was developed using the least squares method:

$$h_{0.01}/d_0 = 1.16q^{0.72}.(x/d_0)^{0.32}\theta^{0.11} \tag{1}$$

Figure 19 demonstrates that, given this definition of penetration height, there is reasonably good agreement between the measured penetration heights and correlation-predicted values for the test conditions in the present study.

Another penetration height correlation, developed by Gruber et al. [11], was also compared with the present measurements. The correlation was developed for air and helium injected from circular and elliptical injectors at 90 deg into a Mach 2 crossflow inside the same wind tunnel based on planar laser scattering from ice particles (that form naturally in the freestream air) to delineate the boundary between the injectant and the freestream air; in particular, the jet boundary was based on a scattering signal of 90% of the average freestream value downstream of the bow shock [11]. The correlation is shown as follows, where d_{eff} is the effective diameter of the injector orifice and r is the effective injector radius:

$$h/(d_{\text{eff}}q) = 1.20((x + r)/(d_{\text{eff}}q))^{0.344} \tag{2}$$

For the present study with the 90 deg round injectors, $d_{\text{eff}} = d_0$. Figure 20 shows a comparison of the measurements and the predictions from Eq. (2). Only the 90 deg jets were used for comparison in Fig. 20. It appears that, except for the highlighted $q = 0.25$ conditions, the predicted penetration height from Eq. (2) is smaller than the present measurement, presumably due to the differences in diagnostics and the definition for penetration height. The observed difference in Fig. 20 can be reduced if the threshold for the definition of penetration height is relaxed to an ethylene mole fraction of 0.10 for the present measurement. As discussed with respect to Fig. 6, the $q = 0.25$ jet is barely choked and may not have a sufficiently high q to emerge from the relatively thick boundary layer. Consequently, the general jet behavior is strongly influenced by the boundary layer and exhibits a noticeable deviation from the other ethylene jets. Nonetheless, Eq. (2) gives consistent predictions for the penetration heights of the present ethylene jets injected at 90 deg, and Eq. (1) extends the treatment to jets injected at 30 deg. Also, the applicability of an existing penetration height correlation should be assessed with

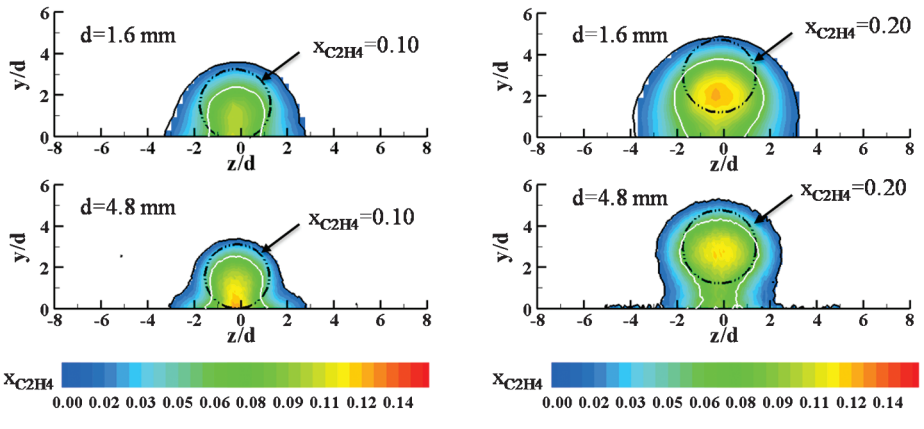

Fig. 18 Ethylene mole fraction contours for ethylene jets injected from 1.6 mm (1/16 in.) and 4.8 mm (3/16 in.) injectors with $x/d = 25$ and $\theta = 90$ deg: a) $q = 0.5$, and b) $q = 1.0$.

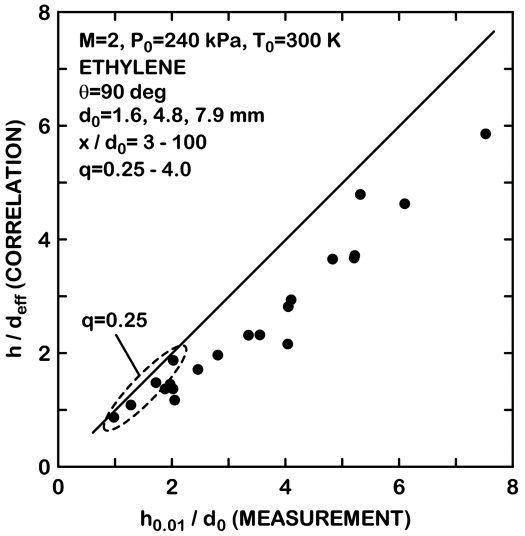

Fig. 20 Comparison of the measured penetration heights and the predictions from Gruber et al. [11], shown here in Eq. (2), for ethylene jets injected at 90 deg.

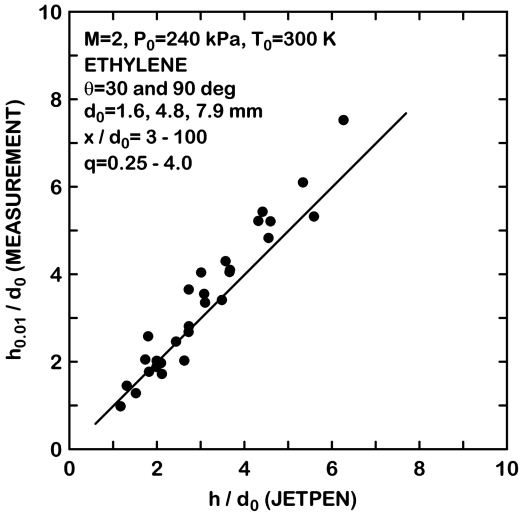

Fig. 21 Comparison of the JETPEN-predicted penetration heights and the measured penetration heights, $h_{0.01}$.

the employed diagnostics and the adopted definition for penetration height in mind. Nonetheless, with the observed discrepancies in the JETPEN-predicted fuel plume structures in Figs. 4–16, the predicted fuel plume penetration heights are generally in good agreement with the measured fuel plume penetration heights based on the 1% mole fraction contour, $h_{0.01}$. Figure 21 further illustrates the agreement.

Conclusions

Structures of ethylene jets injected at 30 and 90 deg from three orifice diameters into a Mach 2 supersonic crossflow were studied experimentally, using Raman scattering to quantify the concentration contours within the fuel plumes at various freestream locations. The ratio of the cross-sectional areas of the largest and smallest injectors is 25:1. The measured quantitative ethylene concentrations were compared with the predictions from the revised JETPEN code, which was calibrated primarily with helium and hydrogen.

It was found that discrepancies between the measurements and the JETPEN predictions for the structures of ethylene fuel plumes were observed. Generally, the JETPEN code underpredicts the fuel plume size for ethylene jets injected at 90 deg. The underprediction is worse at large x/d and especially at conditions of high jet-to-air momentum flux ratio. The JETPEN code slightly overpredicts the fuel plume size for the 30 deg jets. Furthermore, for a given injection condition, the predicted fuel plume for the 30 deg jet is larger than that for the 90 deg jet. This is contradicted by the experimental observation. Despite the observed discrepancies in fuel plume structure, the fuel plume penetration heights predicted by the JETPEN code agree reasonably well with the measured penetration heights, for which a threshold of 0.01 for ethylene mole fraction was used to define the penetration height. Based on the present data set, a new penetration height correlation was developed to treat the cases with injection angles at 30 and 90 deg.

Because of the effects of the wall boundary layer, fuel plume scalability in terms of shape, size, and concentration profiles was demonstrated only with the 4.8 and 7.9 mm injectors, representing an effective ratio of 2.8:1 for the cross-sectional areas of the injector exit orifices. Improved designs for the test apparatus and injectors should be sought to further minimize the influence of the freestream boundary layer in future studies. In addition, root causes for the deficiencies of the JETPEN code in treating the ethylene jets should be explored to further improve its predictions. Finally, the experimental data generated from the present study can compared with the existing penetration height correlations and be used to validate numerical simulations.

Acknowledgments

This study was supported by and performed at Wright–Patterson Air Force Base under the U.S. Air Force contract F33615-03-D-2419-002 with Innovative Scientific Solutions Incorporated (Mark Hsu is the principal investigator). The support for this project is sincerely appreciated. The authors would also like to thank David Schommer and William Terry of Innovative Scientific Solutions Incorporated for their invaluable engineering support and Anna Creese of Taitech for her editorial consultation.

References

[1] Seiner, J. M., Dash, S. M., and Kenzakowski, D. C., "Historical Survey on Enhanced Mixing in Scramjet Engines," *Journal of Propulsion and Power*, Vol. 17, No. 6, 2001, pp. 1273–1286. doi:10.2514/2.5876

[2] Bogdanoff, D. W., "Advanced Injection and Mixing Techniques for Scramjet Combustors," *Journal of Propulsion and Power*, Vol. 10, No. 2, 1994, pp. 183–190. doi:10.2514/3.23728

[3] Schetz, J. A., Weinraub, R. A., and Mahaffey, R. E. Jr., "Supersonic Transverse Injection into a Supersonic Stream," *AIAA Journal*, Vol. 6, No. 5, 1968, pp. 933–934. doi:10.2514/3.4631

[4] Schetz, J. A., Thomas, R. H., and Billig, F. S., "Mixing of Transverse Jets and Wall Jets in Supersonic Flow," *International Union of Theoretical and Applied Mechanics Symposium on Separated Flows and Jets*, Springer–Verlag, Berlin/New York, 1990, pp. 807–837.

[5] Mays, R. B., Thomas, R. H., and Schetz, J. A., "Low Angle Injection into a Supersonic Flow," AIAA Paper 89-2461, July 1989.

[6] Orth, R. C., and Funk, J. A., "An Experimental and Comparative Study of Jet Penetration in Supersonic Flow," *Journal of Spacecraft and Rockets*, Vol. 4, No. 9, 1967, pp. 1236–1242. doi:10.2514/3.29058

[7] Sriram, A. T., and Mathew, J., "Improved Prediction of Plane Transverse Jets in Supersonic Crossflows," *AIAA Journal*, Vol. 44, No. 2, 2006, pp. 405–407. doi:10.2514/1.17114

[8] Ben-Yakar, A., Mungal, M. G., and Hanson, R. K., "Time Evolution and Mixing Characteristics of Hydrogen and Ethylene Transverse Jets in Supersonic Crossflows," *Physics of Fluids*, Vol. 18, 2006, pp. 026101–026101-16. doi:10.1063/1.2139684

[9] Hermanson, J. C., and Winter, M., "Mie Scattering Imaging of a Transverse Sonic Jet in Supersonic Flow," *AIAA Journal*, Vol. 31, No. 1, 1993, pp. 129–132. doi:10.2514/3.11328

[10] Fuller, E. J., Mays, R. B., Thomas, R. H., and Schetz, J. A., "Mixing Studies of Helium in Air at High Supersonic Speeds," *AIAA Journal*,

Vol. 30, No. 9, 1992, pp. 2234–2243.
doi:10.2514/3.11210

[11] Gruber, M. R., Nejad, A. S., Chen, T. H., and Dutton, J. C., "Transverse Injection from Circular and Elliptic Nozzles into a Supersonic Crossflow," *Journal of Propulsion and Power*, Vol. 16, No. 3, 2000, pp. 449–457.
doi:10.2514/2.5609

[12] Billig, F. S., Orth, R. C., and Lasky, M., "A Unified Analysis of Gaseous Jet Penetration," *AIAA Journal*, Vol. 9, No. 6, 1971, pp. 1048–1058.
doi:10.2514/3.49916

[13] Billig, F. S., and Schetz, J., "Analysis of Penetration and Mixing of Gas Jets in Supersonic Cross Flow," AIAA Paper 92-5061, Dec. 1992.

[14] Gruber, M., Donbar, J., Carter, C., and Hsu, K.-Y., "Mixing and Combustion Studies Using Cavity-Based Flameholders in a Supersonic Flow," *Journal of Propulsion and Power*, Vol. 20, No. 5, 2004, pp. 769–778.
doi:10.2514/1.5360

[15] Doster, J., King, P., Gruber, M., Carter, C., Ryan, M., and Hsu, K.-Y., "In-Stream Hypermixer Fueling Pylons in Supersonic Flow," *Journal of Propulsion and Power*, Vol. 25, No. 4, 2009, pp. 885–901.
doi:10.2514/1.40179

[16] Lemmon, E. W., Huber, M. L., and McLinden, M. O., "NIST Standard Reference Database 23: Reference Fluid Thermodynamic and Transport Properties (REFPROP)," Ver. 8.0, National Inst. of Standards and Technology, Standard Reference Data Program, Gaithersburg, MD, 2007.

V. Yang
Editor-in-Chief Emeritus